Inorganic Chemistry

pubs.acs.org/IC Article

Coacervate Formation in Dilute Aqueous Solutions of Inorganic Molecular Clusters with Simple Divalent Countercations

Published as part of Inorganic Chemistry virtual special issue "Forum on Polyoxometalate and Metal-Oxo Chemistry".

Kexing Xiao,[§] Yuqing Yang,[§] Xiaohan Xu, Jennifer E. S. Szymanowski, Yifan Zhou, Ginger E. Sigmon, Peter C. Burns,* and Tianbo Liu*

Cite This: *Inorg. Chem.* 2024, 63, 15331−15339 Read Online

ACCESS | Metrics & More | Article Recommendations | Supporting Information

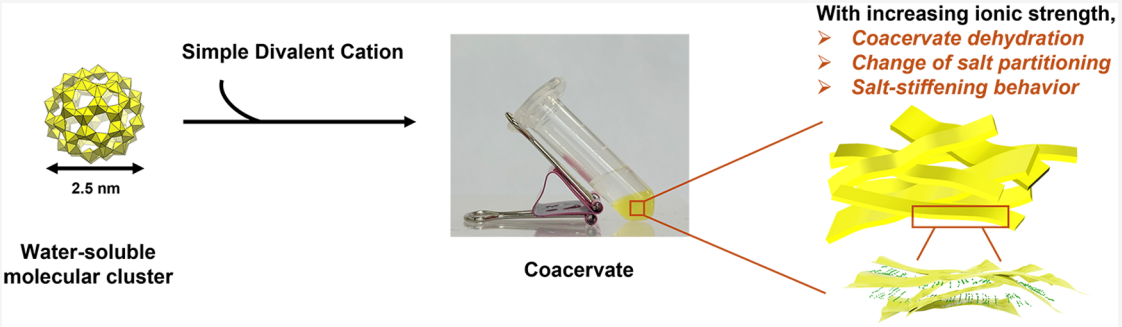

ABSTRACT: We report a complex coacervate formed by a 2.5 nm-diameter, rigid uranyl peroxide molecular cluster ($Li_{68}K_{12}(OH)_{20})[UO_2(O_2)OH]_{60}$, U_{60}^{60-}) and $SrCl_2$ salt in dilute aqueous solutions, including its location in the phase diagram, composition, rheological features, and critical conditions for phase transitions. In this coacervate, the Sr^{2+} cations are a major building component, and the coacervate phase covers a substantial region of the phase diagram. This coacervate demonstrates features that differ from traditional coacervates formed by oppositely charged long-chain polyelectrolytes, especially in its formation mechanism, dehydration, enhancement of mechanical strength with increasing ionic strength, and the change of salt partition preference into the coacervate and supernatant phases with ionic strength.

INTRODUCTION

This paper is dedicated to Professor Achim Müller for his great scientific career. One of the author groups (T.L.) had been extensively collaborating with him for over 20 years. The high-quality, single-crystalline samples provided by Müller's group (mostly discovered by them), such as $\{Mo_{154}\}$, $\{Mo_{176}\}$, $\{Mo_{72}V_{30}\}$, $\{Mo_{72}Cr_{30}\}$, and more, served as nice, valuable models for our early explorations on the uncharted macroionic solutions. The collaborations resulted in new discoveries such as the self-assembly of such macroions into blackberry-type structures,[1,2] the gradual, controllable deprotonation of clusters,[3,4] cation transport inside and outside the shells of Keplerate clusters,[5] etc.[6−11]

While the self-assembly of such clusters was a surprise 20 years ago, our recent studies indicated that their macrophase transitions in dilute aqueous solutions were also unique and complicated. Contradicting to the common understanding that inorganic ions usually possess two macrophasal scenarios in solution if only physical forces are involved—soluble or insoluble (forming amorphous or crystalline structures and precipitate out from solution), we observed macrophase transitions from solution to gel and coacervate phases,[12,13] in the absence of any organic ligand or component, showing that macrophase transition in dilute solutions of inorganic macroions is another area that deserves further studies. Here, we report detailed studies on the coacervate phase formed by a 2.5 nm-size uranyl peroxide molecular cluster, $Li_{48+m}K_{12}(OH)_m[UO_2(O_2)OH]_{60}(H_2O)_n$ ($m \approx 20$ and $n \approx 310$, U_{60}^{60-}),[14] in aqueous solution.

Coacervation is a common liquid−liquid phase separation (LLPS) that usually forms with two oppositely charged polyelectrolytes, yielding a dense macromolecule-rich phase (coacervate phase) and a dilute solution phase (supernatant phase).[15,16] This macrophase separation results in two clearly

Received: May 21, 2024
Revised: July 6, 2024
Accepted: July 15, 2024
Published: August 6, 2024

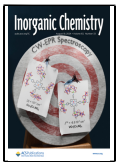

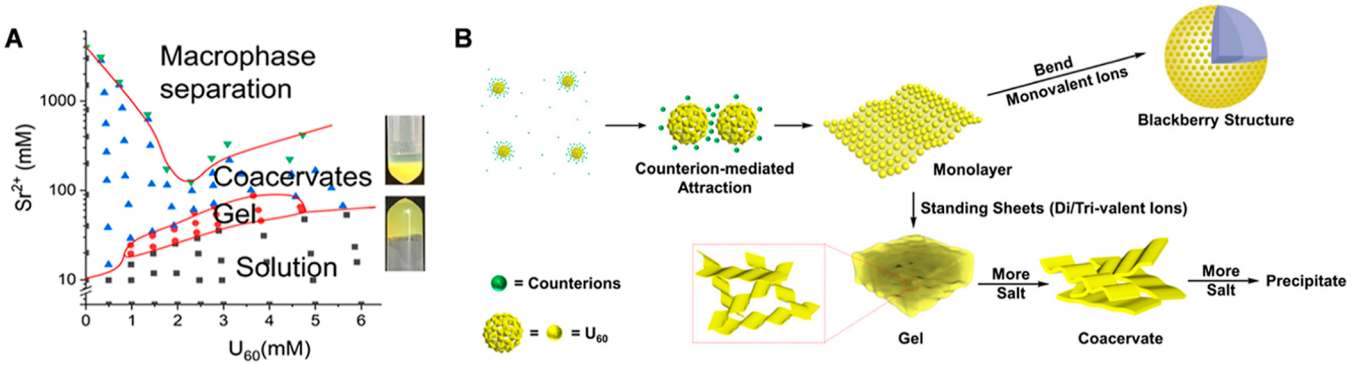

Figure 1. (A) U_{60}^{60-}−$SrCl_2$ binary phase diagram in a dilute aqueous solution. Solution (black squares), gel (red circles), coacervate (blue triangles), and macrophase separation (green inverted triangles) phases with approximate boundaries are shown with photos of the coacervate (right up) and gel (right down). (B) Schematic illustration showing the self-assembly of U_{60}^{60-} with mono-, di-, and trivalent counterions into "blackberry" solutions, gels, or coacervates. Adapted with permission from ref 12. Copyright 2021 American Chemical Society.

distinguished stable liquid phases, with almost all solutes remaining in the coacervate phase. Over the past decade, considerable effort has focused on expanding the scope of coacervation, which now includes any combination of biomolecules (proteins,[17,18] polysaccharides,[19] peptides,[20−23] and polynucleotides[24,25]), colloids,[26] synthetic polymers,[27−30] and surfactants.[31,32] Numerous efforts have been directed toward understanding the physical chemistry underlying coacervation,[33−38] which can be used as an in vitro model to mimic some aspects of membraneless organelles (MLOs).[39−41] Coacervation has been proposed as the mechanism by which MLOs compartmentalize and organize biomolecular processes in our living systems, accounting for "the origin of life".[42]

It is widely thought that the electrostatic interaction (or charge pairing) between oppositely charged groups, associated with the entropy-favored release of counterions, drives coacervate formation.[37,43−45] To maximize the interactions, most coacervation studies have focused on heavily charged macromolecules or macromolecules with many charged units.[27] For example, coacervations in synthetic or biological systems are usually demonstrated between long-chain polyelectrolytes or proteins.[16,19] Notably, the addition of simple salts (e.g., NaCl) is typically required in the coacervation to weaken the bindings between the oppositely charged components.[46] The transformation from coacervate to solution state is normally observed upon adding large amount of salts—the so-called "salt-induced suppression".[47]

Coacervates consisting of low-complexity molecules are also of interest.[48] Recent studies revealed the potential of less complex molecules with lower-molecular-weight or fewer charges as one coacervation component to drive LLPS.[49−51] Mann et al. first reported a complex coacervation combining cationic oligopeptides (<10 monomers) and anionic nucleotides.[20] Keating et al. demonstrated successful LLPSs upon combining one type of macromolecules with oppositely charged small molecules, such as longer polyanionic RNA with a small cationic peptide or organic amine molecules, etc.[22,24,25] In addition to organic molecules, a few studies have exploited small inorganic multivalent ions to mediate the complexation with peptides/RNAs for coacervation.[52−54] At least one component in these coacervates is always long-chain polyelectrolytes, with often inhomogeneous charge distribution. Moreover, the hydrophobic interaction resulting from their nonpolar groups and potential intramolecular interactions originating from their flexible chains inevitably make the mechanism of coacervation complicated. To avoid these, water-soluble inorganic molecular clusters (e.g., polyoxometalates, POMs) that possess rigid configurations, uniform shapes, and known charge distributions[55] were employed for complex coacervation by combination with gelatin,[56] polyzwitterions,[57,58] or short peptides.[59,60] Overall, small organic or inorganic molecules can be used to form complex coacervates, which provide a simple mechanism for the compartmentalization of dilute molecules to generate protocells.

We have recently observed, with the addition of di- or trivalent countercations (e.g., Sr^{2+} and Y^{3+}), two new phases—gels and coacervates—formed in the dilute aqueous solutions of the U_{60}^{60-} cluster (Figure 1).[12] The U_{60}^{60-} molecular macroion has a C_{60}-like spherical structure consisting of 60 uranyl polyhedra that are arranged into 20 hexagons and 12 pentagons and carries 60^- charges (Figure S1).[14] Different from the above-mentioned POM-based coacervates that contain additional organic species, the U_{60}^{60-} divalent cation coacervates comprise only inorganic clusters as macroanions and countercations. Herein, we explore this unconventional coacervation by combining turbidimetry, transmission electron microscopy (TEM), Raman spectroscopy, composition analysis, and rheology techniques. The physical behaviors of this coacervate are remarkably different from conventional complex coacervates in terms of its formation mechanism, composition, structure, and mechanical properties. The structural profile, composition analysis, and viscoelastic response demonstrate an excellent agreement and elucidate an unusual mechanism that captures the intriguing stimuli-responsive behavior of this coacervation system. Noteworthily, as the properties of coacervates formed by U_{60}^{60-} with Sr^{2+} or Ba^{2+} are very similar, the discussions are focused on U_{60}^{60-}−Sr^{2+} coacervates only. The data for U_{60}^{60-}−Ba^{2+} coacervates are shown in the Supporting Information.

MATERIALS AND METHODS

Materials. U_{60}^{60-} cluster crystals were synthesized according to previously reported procedures.[14] Raman spectroscopy and electrospray ionization-mass spectrometry (ESI-MS) characterizations support the successful synthesis of clusters (Figure S2). Strontium chloride hexahydrate and barium chloride dihydrate were purchased from Sigma-Aldrich and used directly without further purification. All water used during the experiment was from a Milli-Q water purification system at 25 °C. All of the experiments were carried out at ambient temperatures unless stated otherwise.

https://doi.org/10.1021/acs.inorgchem.4c02103
Inorg. Chem. 2024, 63, 15331−15339

Sample Preparation. U_{60}^{60-} cluster crystals were dissolved in Milli-Q water in a 2 mL microcentrifuge tube to obtain a U_{60}^{60-} aqueous solution. Concentrated $SrCl_2$ aqueous solution or $SrCl_2$ solid (to avoid the excess dilution of U_{60}^{60-} at a high salt-to-U_{60}^{60-} ratio) was added to the U_{60}^{60-} aqueous solution. The mixture was immediately vortexed for at least 30 s. The concentration of the U_{60}^{60-} aqueous solution (C_{U60}^{60-}) was equal to or smaller than 0.5 mM, where a liquid-to-coacervate transition could be observed depending on the amount of added salt.[12]

Turbidity Measurement. Turbidity measurements were carried out by employing a UV spectrophotometer (Agilent Cary 60) at a wavelength of 570 nm. Neither the U_{60}^{60-} cluster nor strontium chloride absorbs light at this wavelength. After adding $SrCl_2$ to the U_{60}^{60-} aqueous solution in a UV quartz cuvette, the suspension was first mixed by vigorously pipetting at least three times and then quickly conducting the turbidity measurements. The turbidity is defined by $T = -\ln(I/I_0)$, where I_0 is the incident light intensity and I is the intensity of light passed through the sample volume. Triplicate measurements were made for each sample, and the turbidity was recorded in absorption unit (a.u.).

Determination of the Critical Charge Ratio. The charge ratio [+]/[−] is defined as the charges of divalent cation Sr^{2+} over the charges of the U_{60}^{60-} macroanion which carries 60^- charges per cluster. The critical charge ratio ($[+]/[-]_c$) is defined as the charge ratio of divalent cation Sr^{2+} to the U_{60}^{60-} macroanion ([+]/[−]) for coacervation to occur. It was determined upon the gradual addition of divalent salt $SrCl_2$ to the U_{60}^{60-} aqueous solution. For a constant C_{U60}^{60-}, $[+]/[-]_c$ was calculated based on the critical salt concentration at which the solution became turbid, which was confirmed visibly and by turbidimetry (the intersection of two tangents at the start of the significant turbidity increase).

Transmission Electron Microscopy (TEM). TEM images were acquired by utilizing a JEOL-2010 electron microscope operating at 100 kV. In a typical experiment, 3 μL of sample was dropped onto a carbon-coated copper grid and air-dried overnight before imaging.

Raman Spectroscopy. U_{60}^{60-}–Sr^{2+} samples at varied [+]/[−] (~10 μL) were loaded on the glass slide to afford solids after air drying. Raman spectra were collected by using a Renishaw inVia instrument equipped with a thermoelectrically cooled CCD detector and a 785 nm laser source. Statistic scans were taken from wavenumber 600 to 1100 cm^{-1} using 5% laser power with 5 accumulations, 10 s exposure time, and cosmic ray removal.

Coacervate Volume Fraction Measurement. U_{60}^{60-}–Sr^{2+} mixtures were prepared as described in the sample preparation part. The resulting coacervate samples were equilibrated by sitting at room temperature for 48 h, after which the volumes of the coacervate phase did not change. The volumes of the dense coacervate phase after the bulk phase separation were measured using micropipettes. The coacervate volume fraction was calculated based on the ratio of the volume of the coacervate phase to the total volume of the sample mixture.

Dry Weight Analysis of Coacervates. Following the sample preparation protocol, the resulting mixtures were equilibrated for over 48 h. The coacervate phases were collected by carefully removing the supernatant phase via a micropipette. The collected coacervate samples were dried in the oven at 110 °C overnight until obtaining constant masses.[27] Water content or weight percentage of water in the coacervate phase was determined based on the wet weight and dried weight of the coacervate samples. In addition, the amount of remaining $SrCl_2$ salts that exist in the coacervate phase was derived as the mass difference between the dried weight of the coacervate sample and the mass of the remaining U_{60}^{60-} cluster in coacervate (part of the clusters would be broken down after the heating process[14]). Assuming that all of the counterions (K^+, Li^+) would stay in the supernatant phase, the $SrCl_2$ concentration in the coacervate phase can be determined quantitatively.

Rheological Measurements. Dynamic rheology of U_{60}^{60-}–Sr^{2+} coacervates was characterized at ambient temperature by using a TA Instruments DHR-2 strain-controlled rheometer fitted with 8 mm parallel plates. The coacervate samples were prepared based on the preparation protocols at 0.5 mM C_{U60}^{60-} but different charge ratios [+]/[−]. The samples were equilibrated by allowing them to rest at room temperature for 48 h. Afterward, for each sample, the bottom phase was carefully extracted by removing the supernatant layer and then loaded onto the bottom geometry. The gap spacing was kept at 0.5 mm. A strain amplitude sweep test was conducted to determine the linear viscoelastic regions of the samples. After that, an oscillatory frequency sweep was performed from 0.1 to 30 rad/s at a constant strain amplitude of 1%.

RESULTS AND DISCUSSION

U_{60}^{60-}–Sr^{2+} Coacervates in Dilute Aqueous Solutions—Location in the Phase Diagram and Critical Conditions. When the U_{60}^{60-} concentration (C_{U60}^{60-}) is above 0.5 mM, a gel state and a coacervate state are found with increasing $SrCl_2$ concentration (Figure 1).[12] As the focus of this work is to understand the U_{60}^{60-} coacervation, the scope is limited to $C_{U60}^{60-} \leq 0.5$ mM.

We first investigated the critical transition conditions for the formation of U_{60}^{60-}-simple divalent cation coacervates. Upon gradual addition of $SrCl_2$ into a 0.5 mM (~10 mg/mL) U_{60}^{60-} aqueous solution, the mixed solution changes from transparent to cloudy by visual observation. In a few minutes, liquid–liquid phase separation occurs, resulting in a dense, homogeneous, yellow coacervate phase and an upper transparent supernatant phase (Figure 2A). The coacervate phase occurs over a wide range of Sr^{2+} concentrations up to 1.0 M; above that concentration, considerable solid precipitates appear and accumulate at the bottom of the lower phase. For U_{60}^{60-} concentrations lower than 0.5 mM, similar phenomena were also observed when gradually adding $SrCl_2$.

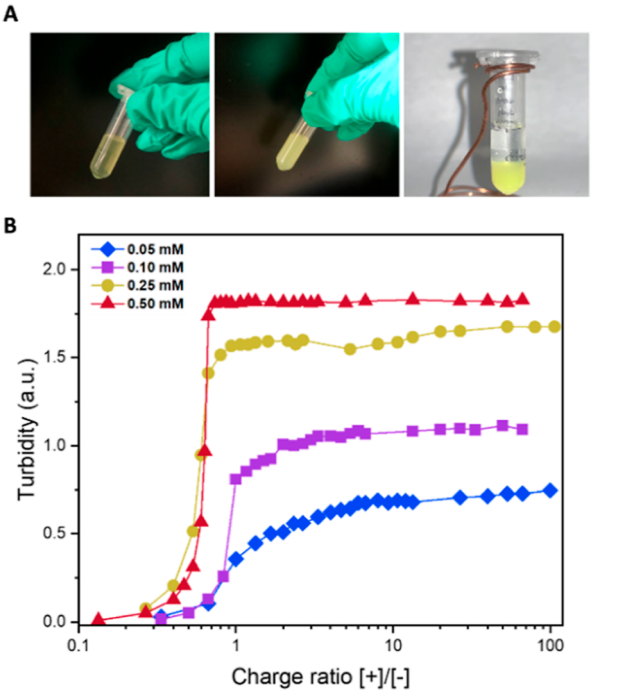

Figure 2. (A) Photographs of U_{60}–Sr^{2+} samples prepared at a 0.5 mM C_{U60}^{60-} with an increased charge ratio of the Sr^{2+} to U_{60}^{60-}macroanion: sample changes from a clear solution to a turbid mixture and eventually undergoes a macroscopic phase separation (from left to right). (B) Turbidity plot as a function of the charge ratio of the Sr^{2+} to U_{60}^{60-} macroanion at 0.05, 0.1, 0.25, and 0.5 mM C_{U60}^{60-}, respectively.

https://doi.org/10.1021/acs.inorgchem.4c02103
Inorg. Chem. 2024, 63, 15331−15339

Scheme 1. Proposed Coacervation Mechanism between U_{60}^{60-} Macroanions (Larger Yellow Spheres) and Sr^{2+} Cations (Smaller Green Spheres) with Increasing Charge Ratio [+]/[−]: The Sample Mixture Persists as a Clear Solution Initially Followed by a Liquid−Liquid Phase Separation

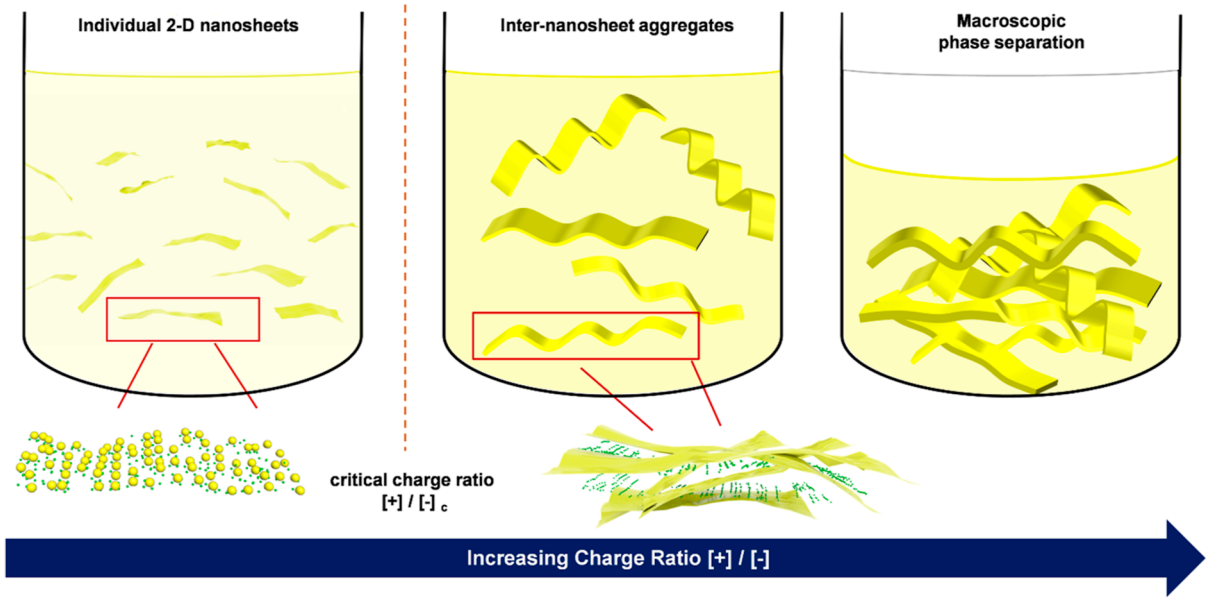

Turbidity measurements were performed to investigate the impact of the charge ratio between Sr^{2+} and U_{60}^{60-} ([+]/[−]) on coacervate formation (Figure 2B). When the U_{60}^{60-} concentration is relatively high (0.25 and 0.5 mM), the initial turbidity of the mixed solution increases slightly until the Sr^{2+}/U_{60}^{60-} charge ratio ([+]/[+]) reaches 0.6, where an abrupt increase in turbidity is observed, corresponding to the formation of a significant amount of coacervates. Above this critical charge ratio ($[+]/[-]_c \sim 0.6$), a turbidity plateau prevails up to [+]/[−] ∼ 100, suggesting a broad coacervation range over Sr^{2+} concentration. Similar trends were observed in U_{60}^{60-} solutions with lower concentrations (0.1 and 0.05 mM) but with a higher critical charge ratio ($[+]/[-]_c \sim 0.8$). Meanwhile, the maximal turbidity is observed at [+]/[−] ∼ 1 for all U_{60}^{60-} concentrations, the situation where Sr^{2+} and U_{60}^{60-} have equivalent total charges. This has also been extensively reported in complex coacervates.[45] Although many complex coacervates appear around the equivalent charge ratio, those coacervates involving rigid cluster macroions often show a broad range of charge ratios,[57,60] including the current one. The U_{60}^{60-} coacervates can be formed over a very broad range of charge ratios up to 100, similar to some RNA-based coacervates in which one of the components has lower multivalency compared to the other.[22,24,25] In addition, as shown in Figure 2A, the maximum turbidity increases from 0.75 to 1.8 with an increasing U_{60}^{60-} concentration from 0.05 to 0.5 mM, implying an increasing amount or size of the coacervate complexes.

Formation Mechanism of U_{60}^{60-}−Sr^{2+} Coacervates. Based on the experimental results described above, a mechanism for the evolution of the unconventional U_{60}^{60-}−Sr^{2+} coacervation is proposed (Scheme 1). The process involves two major stages corresponding to the two states: a clear solution and a turbid suspension followed by liquid−liquid phase separation. First, when the charge ratio is below the critical charge ratio for coacervation ($[+]/[-]_c$), the imbalance between macroanions and Sr^{2+} cations leads to moderate counterion association around U_{60}^{60-} macroanions upon adding Sr^{2+} cations to the solution.[61,62] Molecular dynamics simulation confirms that the consequent counterion-mediated attraction will lead to the formation of two-dimensional (2-D) sheets because the counterions tend to be distributed around the equatorial area of the U_{60}^{60-} macroions with U_{60}^{60-} having one of its topological pentagons facing the bottom (in this way, U_{60}^{60-} has the maximum charge density around its equatorial area).[63,64] These 2-D nanosheets of relatively smaller sizes carry negative charges and thus remain isolated in solution owing to their electrostatic repulsion. At this stage, the U_{60}^{60-}−Sr^{2+} mixture continued to be a transparent solution. With the continuous addition of Sr^{2+}, the nanosheets gradually grow. In the presence of weaker (monovalent) counterions, the sheets will be more flexible and will bend to form hollow, spherical, single-layered blackberry structures (Figure 1B).[65,66] With stronger counterions such as Sr^{2+}, however, the sheets are more rigid. They persist as extended sheets in solution and internanosheet attraction will occur, leading to further aggregation. The less soluble internanosheet aggregates ultimately sediment into a dense coacervate phase, resulting in the macroscopic phase separation at the critical charge ratio $[+]/[-]_c$.

TEM was utilized to characterize the formation and structure of the U_{60}^{60-}−Sr^{2+} coacervates. The formation of large 2-D thin-layered sheets has been identified in U_{60}^{60-} solutions by experimental and simulation approaches and is attributed to the counterion-mediated attraction between Sr^{2+} and U_{60}^{60-} macroions (Figure 1B).[12,64] Herein, thin-film-like nanosheet structures are confirmed for a solution sample prepared at 0.5 mM C_{U60}^{60-} and [+]/[−] = 0.47 by TEM (Figure 3A). With a further increase in $SrCl_2$ concentration, coacervation occurs, and less transparent (darker in the images) and larger nanosheets (Figure 3B, compared with Figure 3A) are observed, which suggests a more compact stacking of nanosheet structures in the U_{60}^{60-}−Sr^{2+} coacervates. In addition, Raman spectroscopy was applied to probe any structural change of the U_{60}^{60-} cluster in the presence of Sr^{2+}. At varied [+]/[−], there are no obvious shifts for the two

https://doi.org/10.1021/acs.inorgchem.4c02103
Inorg. Chem. 2024, 63, 15331−15339

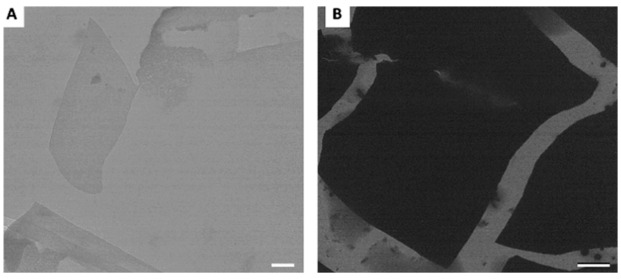

Figure 3. TEM images of the (A) U_{60}^{60-}–Sr^{2+} solution prepared at 0.5 mM C_{U60}^{60-} and [+]/[−] = 0.47 and (B) U_{60}^{60-}–Sr^{2+} coacervate prepared at 0.5 mM C_{U60}^{60-} and [+]/[−] = 0.67. Scale bar: (A) 200 nm, (B) 2 μm.

prominent bands of U_{60}^{60-} that are located at 805 and 842 cm^{-1}, corresponding to the symmetric stretch of the uranyl cation (ν_{O-U-O}) and the peroxo ligand (ν_{O-O}), respectively (Figure S3).[67] The results confirm the integrity of the U_{60}^{60-} macroion that no chemical reaction is involved in U_{60}^{60-}–Sr^{2+} coacervations. The coacervate is formed completely by physical interactions and can be converted back to the solution state through dilution with the retention of thin-film-like sheet structures and structural integrity of the U_{60}^{60-} cluster (Figure S4).

Composition of the U_{60}^{60-}–Sr^{2+} Coacervates. The compositions of U_{60}^{60-}–Sr^{2+} coacervates were determined at different U_{60}^{60-} concentrations and Sr^{2+}/U_{60}^{60-} charge ratios above $[+]/[-]_c$. The yield of the coacervate is determined by the volume fraction of the coacervate phase in the mixture after phase separation. At $[+]/[-]_c$, the maximum coacervate yield is ∼50% at 0.5 mM C_{U60}^{60-} (Figure 4A). When C_{U60}^{60-} in the system decreases to 0.1 mM and the charge stoichiometry reaches about 1:1, the yield of coacervate decreases to ∼16% (Table S2). A colorless supernatant phase and a yellow coacervate phase are always observed after the bulk phase separation, as depicted in Figure 2A, indicating that essentially all of the yellow U_{60}^{60-} macroanions are in the coacervate layer after phase separation. Therefore, it is reasonable to expect that the coacervate yield is lower at smaller C_{U60}^{60-} owing to the smaller amount of U_{60}^{60-} in solution.

Next, we examined the effect of the charge ratio on the yield of coacervates by increasing the amount of added salt at a constant C_{U60}^{60-}. Figure 4A demonstrates the relationship between the volume fraction of coacervates and the charge ratio at 0.5 mM C_{U60}^{60-}, where two regimes can be identified based on the variation of the coacervate yield. In the low-charge ratio regime ($0.6 < [+]/[-] \leq 3.33$), with increasing charge ratio, the volume fraction of coacervates first decreases significantly from ∼50 to ∼28% and then remains ∼28 ± 2% upon further increase of the charge ratio, suggesting that the coacervation reaches a steady state in the high-charge ratio regime ($[+]/[-] > 3.33$). In addition, the "strength" of the coacervation is estimated based on the amount of water expelled from the U_{60}^{60-}–Sr^{2+} coacervate phase. As shown in Figure 4B, at $[+]/[-]_c$, ∼98 wt % of the coacervate phase is water, analogous to the water content in reported hydrophilic polyelectrolyte coacervates.[27,41] Upon increasing the charge ratio, the measured water content dropped dramatically from 98 to 84 wt %, implying that the strength of the coacervation is enhanced at higher salt concentrations. Notably, the dehydration of U_{60}^{60-}–Sr^{2+} coacervates with salt addition is in contrast to the salt-induced suppression of conventional polyelectrolyte coacervates where the water content normally goes up with added salt.[29] Indeed, we contend that the expulsion of water from our U_{60}^{60-}–Sr^{2+} coacervate can be attributed to its salt-stiffening behavior, which is demonstrated in the following section.

To gain further insight into the U_{60}^{60-}–Sr^{2+} coacervates that are formed at different charge ratios, we estimate the distribution of salt ions qualitatively. The concentration of Sr^{2+} in the coacervate phase as a function of the charge ratio [+]/[−] is shown in Figure 5A. With increasing [+]/[−], the Sr^{2+} concentration in the coacervate phase increases. The existence of more Sr^{2+} cations in the coacervate phase at a higher [+]/[−] can bring U_{60}^{60-}–Sr^{2+} nanosheets into closer proximity and repel more water into the supernatant phase. The Sr^{2+} distribution is further quantified by using the salt partition coefficient $P_{c/s}$, which is defined as the ratio of salt concentrations in the coacervate and supernatant phases. At $[+]/[-]_c$, the majority of $SrCl_2$ remains in the coacervate phase with the corresponding $P_{c/s}$ being ∼13. In other words,

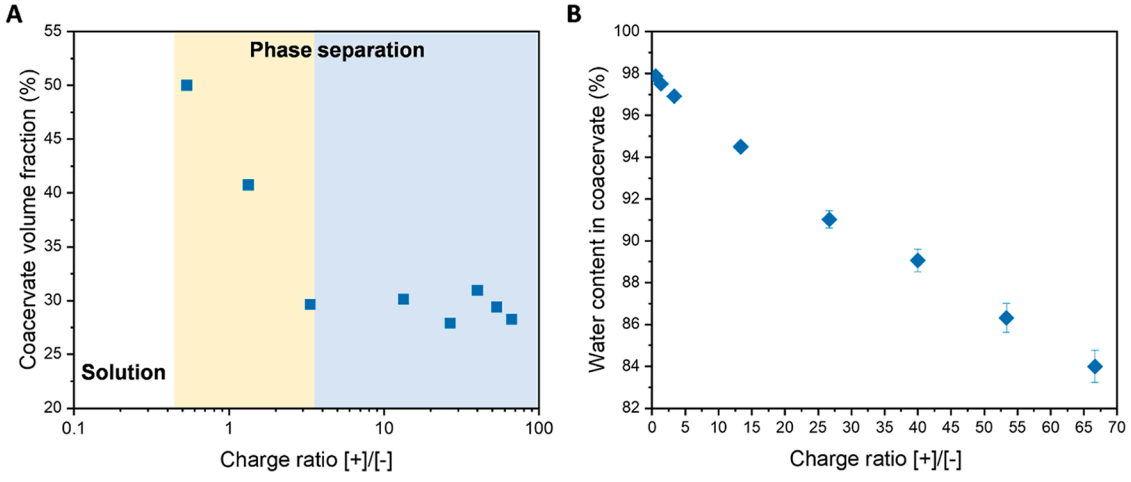

Figure 4. (A) Volume fraction of coacervates indicating the coacervate yield as a function of charge ratio [+]/[−] between added Sr^{2+} cations and U_{60}^{60-} macroanions. Yellow- and blue-highlighted backgrounds represent the low-charge ratio region and high-charge ratio region after bulk phase separation, respectively. (B) Weight percentage of water in the U_{60}^{60-}–Sr^{2+} coacervate phase as a function of charge ratio [+]/[−]. For (A) and (B), the U_{60}^{60-} concentration is fixed at 0.5 mM to prepare coacervate samples.

https://doi.org/10.1021/acs.inorgchem.4c02103
Inorg. Chem. 2024, 63, 15331−15339

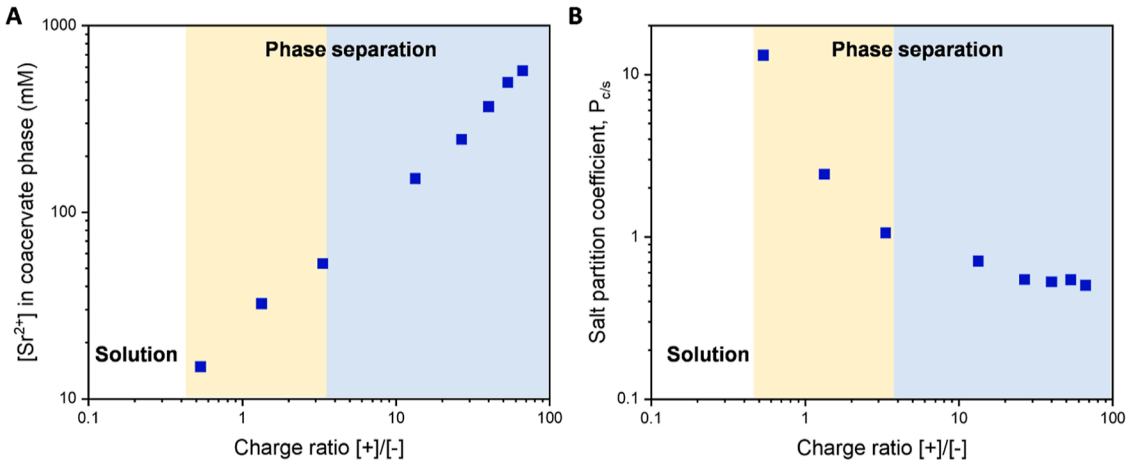

Figure 5. (A) Concentration of $SrCl_2$ (mM) in the coacervate phase as a function of charge ratio [+]/[−] for the U_{60}^{60-}−Sr^{2+} coacervate prepared at 0.5 mM C_{U60}^{60-}. (B) Salt partition coefficient $P_{c/s}$ trends with a charge ratio [+]/[−] for the U_{60}^{60-}−Sr^{2+} coacervate prepared at 0.5 mM C_{U60}^{60-}. Yellow- and blue-highlighted backgrounds represent the low-charge ratio region and high-charge ratio region after bulk phase separation, respectively.

most of the divalent countercations accumulate within the U_{60}^{60-}−Sr^{2+} coacervates at this stage. The ability of compartmentalizing smaller charged molecules (e.g., nucleotides, short peptides, or simple ions) has been greatly emphasized in biological coacervates,[25,68,69] which are believed to facilitate crucial chemical reactions in living cells.[70] Upon further addition of $SrCl_2$, Sr^{2+} exhibits a very intriguing partitioning behavior into either the coacervate or supernatant phase depending on the ionic environment (Figure 5B). In the low-charge ratio regime ($0.6 < [+]/[-] \leq 3.33$), $P_{c/s}$ decreases dramatically as [+]/[−] increases. A value of $P_{c/s}$ over 1.0 indicates the preferential partitioning for Sr^{2+} cations into the coacervate phase. When [+]/[−] > 3.33, $P_{c/s}$ becomes smaller than 1.0, suggesting a transition for Sr^{2+} to preferably partition into the supernatant phase. We speculate that the more significant excluded volume interaction might be responsible for the reversed salt partitioning behavior. With further increasing [+]/[−], $P_{c/s}$ continues to decrease until it approaches a constant value of ∼0.5. The coacervate phase again reaches equilibrium in the high-charge ratio regime. It is noted that the external osmotic pressure from the gradient of salt concentration in different phases has been attributed to the dehydration of polyelectrolyte complexes previously.[71] We contend that it is also a reasonable explanation for the salt-induced water loss observed in our U_{60}^{60-}−Sr^{2+} coacervates formed at high charge ratios. Overall, a responsive partitioning preference for the simple divalent cations, as one component of the U_{60}^{60-}−Sr^{2+} coacervation, is found depending on the ionic environment. Such responsive behavior is unconventional when compared with the synthetic polyelectrolyte coacervates where the salts are normally excluded into the supernatant phase[38] and the biological complex coacervates that normally sequester a large amount of salt ions.[25]

Rheology of the U_{60}^{60-}−Sr^{2+} Coacervates. In addition to understanding the formation mechanism of complex coacervates, extensive studies have been focused on their structures and mechanical properties.[34] Herein, small amplitude oscillatory shear (SAOS) measurements were used to examine the microstructures and mechanical properties of U_{60}^{60-}−Sr^{2+} coacervates. As shown in Figure 6A, for the U_{60}^{60-}−Sr^{2+} coacervate prepared at [+]/[−]$_c$, the storage moduli (G') are larger than the loss moduli (G'') over the

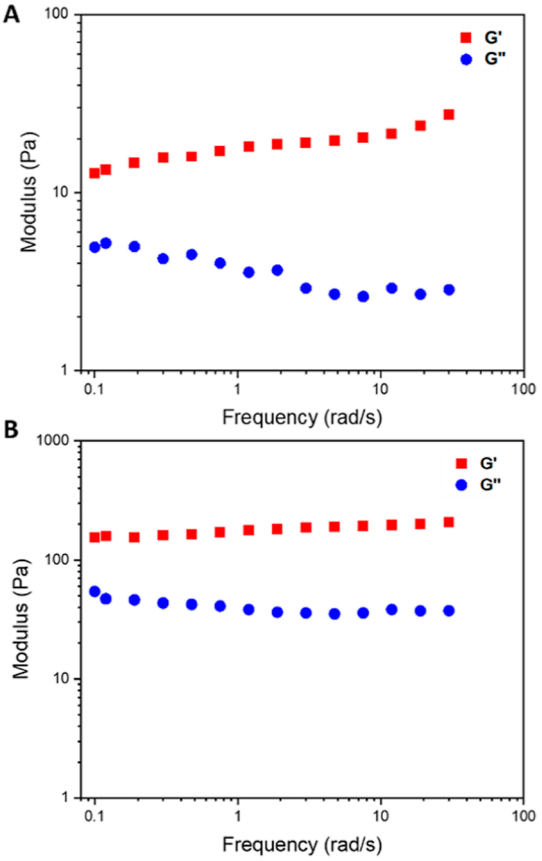

Figure 6. Rheological measurements for the U_{60}^{60-}−Sr^{2+} coacervate prepared at 0.5 mM C_{U60}^{60-} and (A) [+]/[−] = 0.67 or (B) [+]/[−] = 13.3. Red and blue symbols denote the storage (G') and loss (G'') moduli, respectively.

entire measured frequency range and the two moduli are almost independent of the measured frequency. Such a viscoelastic response suggests the formation of a gel-like network structure, which is enabled via the electrostatic attractions between the negatively charged U_{60}^{60-}−Sr^{2+} nanosheets and Sr^{2+} cations with Sr^{2+} serving as the junction points (nodes) (Scheme 1). It is noteworthy that this "soft gel"

https://doi.org/10.1021/acs.inorgchem.4c02103
Inorg. Chem. 2024, 63, 15331−15339

feature is different from the conventional polyelectrolyte complex coacervates that usually exhibit liquid-like viscoelastic features[34] but analogous to some protein−polysaccharide complex coacervates.[72−74] Furthermore, the continued addition of salt can effectively modify the viscoelastic response of the U_{60}^{60-}−Sr^{2+} coacervate (Figure 6B). Distinct from the salt-weakening behavior of conventional synthetic coacervate complexation, we notice that the magnitude of G' increases from ∼20 to ∼200 Pa upon the increase of [+]/[−]. In other words, increasing the salt concentration can considerably enhance the mechanical strength of the U_{60}^{60-}−Sr^{2+} coacervate. Such salt-stiffening behavior again aligns with the composition profile and can be explained based on our proposed model: A larger number of Sr^{2+} cations in the coacervate phase will have stronger electrostatic attractions with the U_{60}^{60-}−Sr^{2+} nanosheets, and the corresponding dehydration of coacervate, altogether, will make the coacervate stiffen, resulting in a more compact and stronger coacervate network.

CONCLUSIONS

We have shown that formation of a complex coacervate can be induced by an inorganic macroanion U_{60}^{60-} and a divalent cation Sr^{2+}. This U_{60}^{60-}−Sr^{2+} coacervate is considerably different from conventional complex coacervates in regard to its composition, formation mechanism, and structural and rheological properties. In the presence of Sr^{2+}, U_{60}^{60-} macroanions can self-assemble into 2-D nanosheet structures via counterion-mediated attraction. Further addition of Sr^{2+} enables the formation of internanosheet aggregates between the negatively charged 2-D nanosheets. As a result, phase separation occurs, and a dense coacervate phase is generated.

By varying the ionic strengths, we have observed interesting salt-responsive properties of the resulting U_{60}^{60-}−Sr^{2+} coacervates. At low ionic strengths, Sr^{2+} countercations preferentially partition into the coacervate phase. The counterion-mediated attraction among the internanosheet aggregates becomes stronger, strengthening the packing of 2-D nanosheets to repel water molecules from the coacervate to the supernatant phase. With the continuous addition of Sr^{2+}, it undergoes a preferable partitioning into the supernatant phase, possibly owing to the stronger excluded volume interaction. Dehydration of the coacervate phase could be induced by osmotic deswelling, while the excess of added Sr^{2+} replaces water molecules that are expelled from the coacervate phase, resulting in the overall equilibrium of the coacervate phase formed at high ionic strength. Rheological measurements reveal a weak gel-like network structure in the U_{60}^{60-}−Sr^{2+} coacervate. At higher ionic strength, the U_{60}^{60-}−Sr^{2+} coacervate is stiffened owing to the above-mentioned dehydration. This uncommon salt-enhancing behavior confirms our proposed model: with larger quantities of countercations, stronger attractions between 2-D nanosheets will lead to the formation of a more compact internanosheet network. Overall, our findings further expand the coacervation scope and demonstrate that coacervation between macroions and simple salts can be a general phenomenon, with features different from conventional coacervates formed by oppositely charged polyions.

ASSOCIATED CONTENT

Supporting Information

The Supporting Information is available free of charge at https://pubs.acs.org/doi/10.1021/acs.inorgchem.4c02103.

Cluster structure, ESI-MS and Raman spectra, calculation summary for the U_{60}^{60-}−Sr^{2+} coacervate, and experimental results for the U_{60}^{60-}−Ba^{2+} coacervate (PDF)

AUTHOR INFORMATION

Corresponding Authors

Peter C. Burns − *Department of Civil and Environmental Engineering and Earth Sciences and Department of Chemistry and Biochemistry, University of Notre Dame, Notre Dame, Indiana 46556, United States;* orcid.org/0000-0002-2319-9628; Email: pburns@nd.edu

Tianbo Liu − *School of Polymer Science and Polymer Engineering, The University of Akron, Akron, Ohio 44325, United States;* orcid.org/0000-0002-8181-1790; Email: tliu@uakron.edu

Authors

Kexing Xiao − *School of Polymer Science and Polymer Engineering, The University of Akron, Akron, Ohio 44325, United States;* orcid.org/0000-0002-3911-342X

Yuqing Yang − *School of Polymer Science and Polymer Engineering, The University of Akron, Akron, Ohio 44325, United States*

Xiaohan Xu − *School of Polymer Science and Polymer Engineering, The University of Akron, Akron, Ohio 44325, United States;* orcid.org/0000-0002-3500-0815

Jennifer E. S. Szymanowski − *Department of Civil and Environmental Engineering and Earth Sciences, University of Notre Dame, Notre Dame, Indiana 46556, United States*

Yifan Zhou − *School of Polymer Science and Polymer Engineering, The University of Akron, Akron, Ohio 44325, United States*

Ginger E. Sigmon − *Department of Civil and Environmental Engineering and Earth Sciences, University of Notre Dame, Notre Dame, Indiana 46556, United States*

Complete contact information is available at: https://pubs.acs.org/10.1021/acs.inorgchem.4c02103

Author Contributions

[§]K.X. and Y.Y. contributed equally.

Notes

The authors declare no competing financial interest.

ACKNOWLEDGMENTS

T.L. acknowledges support from the National Science Foundation (NSF DMR2215190) and the University of Akron. P.C.B. acknowledges support from the University of Notre Dame.

REFERENCES

(1) Liu, T.; Diemann, E.; Li, H.; Dress, A. W. M.; Müller, A. Self-assembly in aqueous solution of wheel-shaped Mo154 oxide clusters into vesicles. *Nature* **2003**, *426* (6962), 59−62.

(2) Liu, T.; Langston, M. L. K.; Li, D.; Pigga, J. M.; Pichon, C.; Todea, A. M.; Müller, A. Self-Recognition Among Different Polyprotic Macroions During Assembly Processes in Dilute Solution. *Science* **2011**, *331* (6024), 1590−1592.

(3) Liu, T.; Imber, B.; Diemann, E.; Liu, G.; Cokleski, K.; Li, H.; Chen, Z.; Müller, A. Deprotonations and Charges of Well-Defined {Mo72Fe30} Nanoacids Simply Stepwise Tuned by pH Allow Control/Variation of Related Self-Assembly Processes. *J. Am. Chem. Soc.* **2006**, *128* (49), 15914−15920.
(4) Kistler, M. L.; Liu, T.; Gouzerh, P.; Todea, A. M.; Müller, A. Molybdenum-oxide based unique polyprotic nanoacids showing different deprotonations and related assembly processes in solution. *Dalton Trans.* **2009**, 5094−5100.
(5) Mishra, P. P.; Pigga, J.; Liu, T. Membranes Based on "Keplerate"-Type Polyoxometalates: Slow, Passive Cation Transportation and Creation of Water Microenvironment. *J. Am. Chem. Soc.* **2008**, *130* (5), 1548−1549.
(6) Todea, A. M.; Merca, A.; Bögge, H.; Glaser, T.; Pigga, J. M.; Langston, M. L. K.; Liu, T.; Prozorov, R.; Luban, M.; Schröder, C.; et al. Porous Capsules {(M)M5}12FeIII30 (M = MoVI, WVI): Sphere Surface Supramolecular Chemistry with 20 Ammonium Ions, Related Solution Properties, and Tuning of Magnetic Exchange Interactions. *Angew. Chem., Int. Ed.* **2010**, *49* (3), 514−519.
(7) Müller, A.; Merca, A.; Al-Karawi, A. J. M.; Garai, S.; Bögge, H.; Hou, G.; Wu, L.; Haupt, E. T. K.; Rehder, D.; Haso, F.; et al. Chemical Adaptability: The Integration of Different Kinds of Matter into Giant Molecular Metal Oxides. *Chem.—Eur. J.* **2012**, *18* (51), 16310−16318.
(8) Garai, S.; Merca, A.; Bhowmik, S.; El Moll, H.; Li, H.; Haso, F.; Nogueira, H.; Liu, T.; Wu, L.; Gouzerh, P.; et al. Hedgehog-shaped {Mo368} cluster: unique electronic/structural properties, surfactant encapsulation and related self-assembly into vesicles and films. *Soft Matter* **2015**, *11* (12), 2372−2378.
(9) Liu, T.; Diemann, E.; Müller, A. Hydrophilic Inorganic Macro-Ions in Solution: Unprecedented Self-Assembly Emerging from Historical & Blue Waters. *J. Chem. Educ.* **2007**, *84*, 526.
(10) Schaffer, C.; Merca, A.; Bogge, H.; Todea, A. M.; Kistler, M. L.; Liu, T.; Thouvenot, R.; Gouzerh, P.; Müller, A. Unprecedented and Differently Applicable Pentagonal Units in a Dynamic Library: A Keplerate of the Type $\{(W)W_5\}_{12}\{Mo_2\}_{30}$. *Angew. Chem., Int. Ed.* **2009**, *48*, 149−153.
(11) Müller, A.; Bogge, H.; Sousa, F. L.; Schmidtmann, M.; Kurth, D. G.; Volkmer, D.; van Slageren, J.; Dressel, M.; Kistler, M. L.; Liu, T. Nanometer-Sized Molybdenum-Iron Oxide Capsule-Surface Modifications: External and Internal. *Small* **2007**, *3*, 986−992.
(12) Yang, Y.; Zhou, Y.; Chen, J.; Kohlgruber, T.; Smith, T.; Zheng, B.; Szymanowski, J. E. S.; Burns, P. C.; Liu, T. Standalone 2-D Nanosheets and the Consequent Hydrogel and Coacervate Phases Formed by 2.5 nm Spherical U60 Molecular Clusters in Dilute Aqueous Solution. *J. Phys. Chem. B* **2021**, *125* (44), 12392−12397.
(13) Xu, X.; Yang, Y.; Zhou, Y.; Xiao, K.; Szymanowski, J. E. S.; Sigmon, G. E.; Burns, P. C.; Liu, T. Critical Conditions Regulating the Gelation in Macroionic Cluster Solutions. *Adv. Sci.* **2024**, *11*, 2308902.
(14) Sigmon, G. E.; Unruh, D. K.; Ling, J.; Weaver, B.; Ward, M.; Pressprich, L.; Simonetti, A.; Burns, P. C. Symmetry versus Minimal Pentagonal Adjacencies in Uranium-Based Polyoxometalate Fullerene Topologies. *Angew. Chem., Int. Ed.* **2009**, *48* (15), 2737−2740.
(15) De Jong, H. B.; Kruyt, H. J. R. K. *Colloid Science*; Elsevier: Amsterdam, 1949.
(16) Gucht, J. v. d.; Spruijt, E.; Lemmers, M.; Cohen Stuart, M. A. Polyelectrolyte complexes: Bulk phases and colloidal systems. *J. Colloid Interface Sci.* **2011**, *361* (2), 407−422.
(17) Cooper, C. L.; Dubin, P. L.; Kayitmazer, A. B.; Turksen, S. Polyelectrolyte−protein complexes. *Curr. Opin. Colloid Interface Sci.* **2005**, *10* (1−2), 52−78.
(18) de Kruif, C. G.; Weinbreck, F.; de Vries, R. Complex coacervation of proteins and anionic polysaccharides. *Curr. Opin. Colloid Interface Sci.* **2004**, *9* (5), 340−349.
(19) Turgeon, S. L.; Schmitt, C.; Sanchez, C. Protein−polysaccharide complexes and coacervates. *Curr. Opin. Colloid Interface Sci.* **2007**, *12* (4−5), 166−178.
(20) Koga, S.; Williams, D. S.; Perriman, A. W.; Mann, S. Peptide−nucleotide microdroplets as a step towards a membrane-free protocell model. *Nat. Chem.* **2011**, *3* (9), 720−724.
(21) Perry, S. L.; Leon, L.; Hoffmann, K. Q.; Kade, M. J.; Priftis, D.; Black, K. A.; Wong, D.; Klein, R. A.; Pierce, C. F.; Margossian, K. O.; et al. Chirality-selected phase behaviour in ionic polypeptide complexes. *Nat. Commun.* **2015**, *6* (1), 6052.
(22) Aumiller, W. M.; Keating, C. D. Phosphorylation-mediated RNA/peptide complex coacervation as a model for intracellular liquid organelles. *Nat. Chem.* **2016**, *8* (2), 129−137.
(23) Nakashima, K. K.; Baaij, J. F.; Spruijt, E. Reversible generation of coacervate droplets in an enzymatic network. *Soft Matter* **2018**, *14* (3), 361−367.
(24) Aumiller, W. M.; Pir Cakmak, F.; Davis, B. W.; Keating, C. D. RNA-Based Coacervates as a Model for Membraneless Organelles: Formation, Properties, and Interfacial Liposome Assembly. *Langmuir* **2016**, *32* (39), 10042−10053.
(25) Frankel, E. A.; Bevilacqua, P. C.; Keating, C. D. Polyamine/Nucleotide Coacervates Provide Strong Compartmentalization of Mg2+, Nucleotides, and RNA. *Langmuir* **2016**, *32* (8), 2041−2049.
(26) Kizilay, E.; Kayitmazer, A. B.; Dubin, P. L. Complexation and coacervation of polyelectrolytes with oppositely charged colloids. *Adv. Colloid Interface Sci.* **2011**, *167* (1−2), 24−37.
(27) Spruijt, E.; Westphal, A. H.; Borst, J. W.; Cohen Stuart, M. A.; van der Gucht, J. Binodal Compositions of Polyelectrolyte Complexes. *Macromolecules* **2010**, *43* (15), 6476−6484.
(28) Chollakup, R.; Smitthipong, W.; Eisenbach, C. D.; Tirrell, M. Phase Behavior and Coacervation of Aqueous Poly(acrylic acid)−Poly(allylamine) Solutions. *Macromolecules* **2010**, *43* (5), 2518−2528.
(29) Wang, Q.; Schlenoff, J. B. The Polyelectrolyte Complex/Coacervate Continuum. *Macromolecules* **2014**, *47* (9), 3108−3116.
(30) Rumyantsev, A. M.; Zhulina, E. B.; Borisov, O. V. Complex Coacervate of Weakly Charged Polyelectrolytes: Diagram of States. *Macromolecules* **2018**, *51* (10), 3788−3801.
(31) Wang, Y.; Kimura, K.; Huang, Q.; Dubin, P. L.; Jaeger, W. J. M. Effects of salt on polyelectrolyte− micelle coacervation. *Macromolecules* **1999**, *32* (21), 7128−7134.
(32) Hu, D.; Chou, K. C. Re-Evaluating the Surface Tension Analysis of Polyelectrolyte-Surfactant Mixtures Using Phase-Sensitive Sum Frequency Generation Spectroscopy. *J. Am. Chem. Soc.* **2014**, *136* (43), 15114−15117.
(33) Hoffmann, K. Q.; Perry, S. L.; Leon, L.; Priftis, D.; Tirrell, M.; de Pablo, J. J. A molecular view of the role of chirality in charge-driven polypeptide complexation. *Soft Matter* **2015**, *11* (8), 1525−1538.
(34) Liu, Y.; Winter, H. H.; Perry, S. L. Linear viscoelasticity of complex coacervates. *Adv. Colloid Interface Sci.* **2017**, *239*, 46−60.
(35) Radhakrishna, M.; Basu, K.; Liu, Y.; Shamsi, R.; Perry, S. L.; Sing, C. E. Molecular Connectivity and Correlation Effects on Polymer Coacervation. *Macromolecules* **2017**, *50* (7), 3030−3037.
(36) Lu, T.; Spruijt, E. Multiphase Complex Coacervate Droplets. *J. Am. Chem. Soc.* **2020**, *142* (6), 2905−2914.
(37) Fu, J.; Schlenoff, J. B. Driving Forces for Oppositely Charged Polyion Association in Aqueous Solutions: Enthalpic, Entropic, but Not Electrostatic. *J. Am. Chem. Soc.* **2016**, *138* (3), 980−990.
(38) Li, L.; Srivastava, S.; Andreev, M.; Marciel, A. B.; de Pablo, J. J.; Tirrell, M. V. Phase Behavior and Salt Partitioning in Polyelectrolyte Complex Coacervates. *Macromolecules* **2018**, *51* (8), 2988−2995.
(39) Milin, A. N.; Deniz, A. A. Reentrant Phase Transitions and Non-Equilibrium Dynamics in Membraneless Organelles. *Biochemistry* **2018**, *57* (17), 2470−2477.
(40) van Lente, J. J.; Claessens, M. M. A. E.; Lindhoud, S. Charge-Based Separation of Proteins Using Polyelectrolyte Complexes as Models for Membraneless Organelles. *Biomacromolecules* **2019**, *20* (10), 3696−3703.
(41) Yewdall, N. A.; André, A. A.; Lu, T.; Spruijt, E. Coacervates as models of membraneless organelles. *Curr. Opin. Colloid Interface Sci.* **2021**, *52*, 101416.
(42) Oparin, A. I. *The Origin of Life on the Earth*, 3rd ed.; Oliver & Boyd: London, 1957.

https://doi.org/10.1021/acs.inorgchem.4c02103
Inorg. Chem. 2024, 63, 15331−15339

(43) Priftis, D.; Laugel, N.; Tirrell, M. Thermodynamic Characterization of Polypeptide Complex Coacervation. *Langmuir* **2012**, *28* (45), 15947−15957.
(44) Sing, C. E. Development of the modern theory of polymeric complex coacervation. *Adv. Colloid Interface Sci.* **2017**, *239*, 2−16.
(45) Sing, C. E.; Perry, S. L. Recent progress in the science of complex coacervation. *Soft Matter* **2020**, *16* (12), 2885−2914.
(46) Perry, S. L.; Li, Y.; Priftis, D.; Leon, L.; Tirrell, M. The Effect of Salt on the Complex Coacervation of Vinyl Polyelectrolytes. *Polymers* **2014**, *6* (6), 1756−1772.
(47) Overbeek, J. T. G.; Voorn, M. J. Phase separation in polyelectrolyte solutions. Theory of complex coacervation. *J. Cell. Comp. Physiol.* **1957**, *49* (S1), 7−26.
(48) Ruiz-Mirazo, K.; Briones, C.; de la Escosura, A. Prebiotic Systems Chemistry: New Perspectives for the Origins of Life. *Chem. Rev.* **2014**, *114* (1), 285−366.
(49) Yang, M.; Digby, Z. A.; Chen, Y.; Schlenoff, J. B. Valence-induced jumps in coacervate properties. *Sci. Adv.* **2022**, *8* (20), No. eabm4783.
(50) Cakmak, F. P.; Choi, S.; Meyer, M. O.; Bevilacqua, P. C.; Keating, C. D. Prebiotically-relevant low polyion multivalency can improve functionality of membraneless compartments. *Nat. Commun.* **2020**, *11* (1), 5949.
(51) Kim, H.; Jeon, B.-j.; Kim, S.; Jho, Y.; Hwang, D. S. Upper Critical Solution Temperature (UCST) Behavior of Coacervate of Cationic Protamine and Multivalent Anions. *Polymers* **2019**, *11* (4), 691.
(52) Onuchic, P. L.; Milin, A. N.; Alshareedah, I.; Deniz, A. A.; Banerjee, P. R. Divalent cations can control a switch-like behavior in heterotypic and homotypic RNA coacervates. *Sci. Rep.* **2019**, *9* (1), 12161.
(53) Boeynaems, S.; Bogaert, E.; Kovacs, D.; Konijnenberg, A.; Timmerman, E.; Volkov, A.; Guharoy, M.; De Decker, M.; Jaspers, T.; Ryan, V. H.; et al. Phase Separation of C9orf72 Dipeptide Repeats Perturbs Stress Granule Dynamics. *Mol. Cell* **2017**, *65* (6), 1044.
(54) Wang, X.; Shi, C.; Mo, J.; Xu, Y.; Wei, W.; Zhao, J. An Inorganic Biopolymer Polyphosphate Controls Positively Charged Protein Phase Transitions. *Angew. Chem., Int. Ed.* **2020**, *59* (7), 2679−2683.
(55) Pope, M. T.; Müller, A. Polyoxometalate Chemistry: An Old Field with New Dimensions in Several Disciplines. *Angew. Chem., Int. Ed. Engl.* **1991**, *30* (1), 34−48.
(56) Carn, F.; Steunou, N.; Djabourov, M.; Coradin, T.; Ribot, F.; Livage, J. First example of biopolymer−polyoxometalate complex coacervation in gelatin−decavanadate mixtures. *Soft Matter* **2008**, *4* (4), 735−738.
(57) Jing, B.; Qiu, J.; Zhu, Y. Organic−inorganic macroion coacervate complexation. *Soft Matter* **2017**, *13* (28), 4881−4889.
(58) Jing, B.; Ferreira, M.; Gao, Y.; Wood, C.; Li, R.; Fukuto, M.; Liu, T.; Zhu, Y. Unconventional Complex Coacervation between Neutral Polymer and Inorganic Polyoxometalate in Aqueous Solution via Direct Water Mediation. *Macromolecules* **2019**, *52* (21), 8275−8284.
(59) Xu, J.; Li, X.; Li, J.; Li, X.; Li, B.; Wang, Y.; Wu, L.; Li, W. Wet and Functional Adhesives from One-Step Aqueous Self-Assembly of Natural Amino Acids and Polyoxometalates. *Angew. Chem., Int. Ed.* **2017**, *56* (30), 8731−8735.
(60) Liu, X.; Xie, X.; Du, Z.; Li, B.; Wu, L.; Li, W. Aqueous self-assembly of arginine and K8SiW11O39: fine-tuning the formation of a coacervate intended for sprayable anticorrosive coatings. *Soft Matter* **2019**, *15* (45), 9178−9186.
(61) Misra, A.; Kozma, K.; Streb, C.; Nyman, M. Beyond Charge Balance: Counter-Cations in Polyoxometalate Chemistry. *Angew. Chem., Int. Ed.* **2020**, *59* (2), 596−612.
(62) Chen, J.; Bera, M. K.; Li, H.; Yang, Y.; Sun, X.; Luo, J.; Baughman, J.; Liu, C.; Yao, X.; Chuang, S. S. C.; et al. Accurate Determination of the Quantity and Spatial Distribution of Counter-ions around a Spherical Macroion. *Angew. Chem., Int. Ed.* **2021**, *60* (11), 5833−5837.
(63) Liu, Z.; Liu, T.; Tsige, M. Elucidating the Origin of the Attractive Force among Hydrophilic Macroions. *Sci. Rep.* **2016**, *6* (1), 26595.
(64) Liu, Z.; Liu, T.; Tsige, M. Unique Symmetry-Breaking Phenomenon during the Self-assembly of Macroions Elucidated by Simulation. *Sci. Rep.* **2018**, *8* (1), 13076.
(65) Gao, Y.; Haso, F.; Szymanowski, J. E. S.; Zhou, J.; Hu, L.; Burns, P. C.; Liu, T. Selective Permeability of Uranyl Peroxide Nanocages to Different Alkali Ions: Influences from Surface Pores and Hydration Shells. *Chem. —Eur. J.* **2015**, *21* (51), 18785−18790.
(66) Soltis, J. A.; Wallace, C. M.; Penn, R. L.; Burns, P. C. Cation-Dependent Hierarchical Assembly of U60 Nanoclusters into Macro-Ion Assemblies Imaged via Cryogenic Transmission Electron Microscopy. *J. Am. Chem. Soc.* **2016**, *138* (1), 191−198.
(67) McGrail, B. T.; Sigmon, G. E.; Jouffret, L. J.; Andrews, C. R.; Burns, P. C. Raman Spectroscopic and ESI-MS Characterization of Uranyl Peroxide Cage Clusters. *Inorg. Chem.* **2014**, *53* (3), 1562−1569.
(68) Dora Tang, T. Y.; Rohaida Che Hak, C.; Thompson, A. J.; Kuimova, M. K.; Williams, D. S.; Perriman, A. W.; Mann, S. Fatty acid membrane assembly on coacervate microdroplets as a step towards a hybrid protocell model. *Nat. Chem.* **2014**, *6* (6), 527−533.
(69) Choi, S.; Meyer, M. O.; Bevilacqua, P. C.; Keating, C. D. Phase-specific RNA accumulation and duplex thermodynamics in multiphase coacervate models for membraneless organelles. *Nat. Chem.* **2022**, *14* (10), 1110−1117.
(70) Nott, T. J.; Craggs, T. D.; Baldwin, A. J. Membraneless organelles can melt nucleic acid duplexes and act as biomolecular filters. *Nat. Chem.* **2016**, *8* (6), 569−575.
(71) Meng, S.; Ting, J. M.; Wu, H.; Tirrell, M. V. Solid-to-Liquid Phase Transition in Polyelectrolyte Complexes. *Macromolecules* **2020**, *53* (18), 7944−7953.
(72) Wang, X.; Lee, J.; Wang, Y.-W.; Huang, Q. Composition and Rheological Properties of β-Lactoglobulin/Pectin Coacervates: Effects of Salt Concentration and Initial Protein/Polysaccharide Ratio. *Biomacromolecules* **2007**, *8* (3), 992−997.
(73) Ru, Q.; Wang, Y.; Lee, J.; Ding, Y.; Huang, Q. Turbidity and rheological properties of bovine serum albumin/pectin coacervates: Effect of salt concentration and initial protein/polysaccharide ratio. *Carbohydr. Polym.* **2012**, *88* (3), 838−846.
(74) Liu, J.; Shim, Y. Y.; Shen, J.; Wang, Y.; Reaney, M. J. T. Whey protein isolate and flaxseed (*Linum usitatissimum* L.) gum electrostatic coacervates: Turbidity and rheology. *Food Hydrocolloids* **2017**, *64*, 18−27.

https://doi.org/10.1021/acs.inorgchem.4c02103
Inorg. Chem. 2024, 63, 15331−15339